

PCCP

Accepted Manuscript

Downloaded by Universitat Ulm on 27 June 2012
Published on 23 May 2012 on http://pubs.rsc.org | doi:10.1039/C2CP90000G



This is an *Accepted Manuscript*, which has been through the RSC Publishing peer review process and has been accepted for publication.

Accepted Manuscripts are published online shortly after acceptance, which is prior to technical editing, formatting and proof reading. This free service from RSC Publishing allows authors to make their results available to the community, in citable form, before publication of the edited article. This *Accepted Manuscript* will be replaced by the edited and formatted *Advance Article* as soon as this is available.

To cite this manuscript please use its permanent Digital Object Identifier (DOI®), which is identical for all formats of publication.

More information about *Accepted Manuscripts* can be found in the [Information for Authors](#).

Please note that technical editing may introduce minor changes to the text and/or graphics contained in the manuscript submitted by the author(s) which may alter content, and that the standard [Terms & Conditions](#) and the [ethical guidelines](#) that apply to the journal are still applicable. In no event shall the RSC be held responsible for any errors or omissions in these *Accepted Manuscript* manuscripts or any consequences arising from the use of any information contained in them.

The role of surface defects on large organic molecule adsorption:

Substrate configuration effects

Thomas Waldmann¹, Christina Nenon¹, Katrin Tonigold², Harry E. Hoster^{1,#},

Axel Groß², R. Jürgen Behm^{1,*}

¹Institute of Surface Chemistry and Catalysis, Ulm University, D-89069 Ulm, Germany

²Institute of Theoretical Chemistry, Ulm University, D-89069 Ulm, Germany

ABSTRACT

The role of the configuration of metal surface atoms in the interaction between individual large, planar organic molecules and a metal substrate was investigated by low-temperature scanning tunneling microscopy and density functional theory calculations, including a semi-empirical correction scheme to account for dispersion effects. As test case, we used the adsorption of the oligopyridine derivative 2-phenyl-4,6-bis(6-(pyridine-2-yl)-4-(pyridine-4-yl)pyridine-2-yl)pyrimidine (2,4'-BTP) on a stepped Ag(100) surface. Both experiment, via statistical evaluation of the adsorption site and orientation of 2,4'-BTP ad molecules, and theory indicate distinct structural effects. The results are compared with the adsorption behavior of pyridine derivatives and benzene on metal surfaces. Consequences on the understanding of the interaction between heteroatoms or functional groups in large organic adsorbates and metal atoms in typical nano-scaled surface defects and hence of the interaction with more realistic metal surfaces are discussed.

Keywords: Adsorption, Adsorption site configuration, Structure, Large organic molecules, Molecule-surface interactions, Scanning tunneling microscopy, Density functional theory, Ag(100)

Resubmitted to PCCP: 03.05.2012

* author, to whom correspondence should be addressed: E-mail: juergen.behm@uni-ulm.de

pres. address: TUM CREATE Centre for Electromobility, Singapore 637459

INTRODUCTION

Supramolecular organic assemblies provide a promising class of materials that can be used in a variety of applications such as organic sensors, LEDs, transistors or solar cells.^{1,2} In order to specifically tailor their structural, chemical, physical, electronic properties, a fundamental microscopic understanding of the crucial factors underlying these properties is needed, which can for example be gained by studying well-defined two-dimensional (2D) supramolecular structures. For this reason, supramolecular structures and structure formation of large organic molecules on single crystalline surfaces have been intensely studied during the last two decades.³⁻⁵ Detailed structural information obtained from (partly temperature dependent) scanning tunneling microscopy (STM) studies, in combination with theoretical work, provided a sound basis for the understanding of the energetic driving force responsible for these structures, and it is generally accepted that a subtle balance between molecule-molecule and molecule-substrate interactions is responsible for the self-assembly of these molecules in ordered 2D structures.^{3,6-12} Most of these studies, however, concentrated on structure formation on idealized surfaces, i.e., on extended atomically smooth terraces, while the role of defects such as steps and kinks, which are abundant on more realistic surfaces, has found little interest, despite of its practical relevance in applications and despite of their often higher affinity to adsorbates compared to smooth terraces.^{6,10-13}

This is topic of the present paper, where we elucidate general principles of the interaction of large organic molecules with steps and kinks, using the adsorption of the planar oligopyridine 2,4'-BTP (2-phenyl-4,6-bis(6-(pyridine-2-yl)-4-(pyridine-4-yl)pyridine-2-yl)pyrimidine)¹⁴ on Ag(100) (see Figure 1) as example. Recently, we had examined the same surface/adsorbate system, focusing on the growth of ordered structures.¹⁵ In this paper the occupation of specific adsorption sites with defined atomic configurations, at steps and defects, is quantitatively evaluated by STM measurements, followed by an analysis of the rotational orientation of the

molecules and their association with adsorption at specific kink site configurations. Comparison with the results of dispersion corrected density functional theory (DFT-D) calculations on the adsorption of behavior of pyridine derivatives and benzene, which are similar to the phenyl and pyridyl moieties in 2,4'-BTP, on stepped Ag(100) surfaces, provide further insight into the nature of the relevant interactions. Finally, the results are discussed with findings on the structure of 2D ordered 2,4'-BTP adlayers on Ag(100) terraces.

RESULTS AND DISCUSSION

Up to a coverage of $\sim 0.07 \text{ nm}^{-2}$ (molecules per nm^2), the 2,4'-BTP molecules were found to exclusively adsorb at step edges. This preference is due to the stronger adsorption at low coordinated sites,¹³ which has been observed for many other adsorption systems.^{6,10-12,16} Most striking structural features of the molecules adsorbed at steps are the small bright dots on the upper side of the step edge close to each molecule (see Figure 2a). Closer inspection of the STM data reveals that these protrusions most likely represent one of the peripheral rings (phenyl or pyridyl) of the 2,4'-BTP molecules, which is located on the upper terrace (see also the molecule marked as F in Figure 2a). This is supported by height profiles as the one in Figure 2b, which belongs to the dashed white line in Figure 2a. The height profile represents the apparent position of the STM tip, which is higher if the tip is located over an 2,4'-BTP adsorbate or a Ag(100) terrace that is above a rising step. For further explanation, we use the points A-E throughout in Figure 2. Points B and E are related to 2,4'-BTP adsorbates on the lower or upper terrace, respectively. They have the same apparent height of $\sim 0.15 \text{ nm}$ with respect to the lower (A) and upper (D) Ag(100) terrace. The molecules E on the upper terrace and the protrusions C have very similar apparent heights. Therefore, protrusion C most likely belongs to one of the peripheral rings, and this ring has a similar vertical distance to the upper terrace as the rest of the molecule with respect to the lower one. This would mean that the 2,4'-BTP molecules are

actually lying across the step edges, as illustrated in Figure 2c. Similar to the behavior reported previously for some other polyaromatic adsorbates^{10,11} or graphene monolayers on metal surfaces.^{17,18} It should be noted that the same behavior can also be observed for 2,4'-BTP on Au(111) at low coverages (see inset of Figure 2a).

Visual inspection of STM images such as those shown in Figures 2a or Figure 3b reveals that the rotational alignment of the molecules with respect to the steps is not at all arbitrary. Figure 3a shows the results of a statistical evaluation of the orientations of 250 molecules, which are grouped according to the schemes shown in Figures 3c and 3d. A first set of configurations X_i includes molecules reaching across the steps, which are identified by the characteristic protrusion in the upper terrace ring, while in another set Λ_i , the entire molecule rests on the lower terrace and attaches to the ascending step. The phenyl rings, which are coordinated to metal atoms of the upper terrace, have the same apparent height as molecules located on the lower terrace. Among the step crossing configurations, the orientation X_3 is by far the most favorable one (~79 %). In this configuration, only the phenyl ring rests on the upper terrace, while the remaining part of the molecule is adsorbed on the lower terrace. About 7% of the molecules are found in other step crossing configurations (X_i), while the remaining 14% are distributed over configurations Λ_i , solely adsorbed on the lower terrace. Here we observe a preference for configurations, where at least one of the peripheral pyridyl rings is in touch with the ascending step edge. Specifically, this is the case for configurations Λ_1 , Λ_4 and Λ_5 (see Figures 4a,b), which together account for ~90% of the Λ_i alignments (see inset of Figure 3a). This preference can be explained by an interaction between the N atom and the Ag atoms of the ascending step, in accordance with findings in the DFT calculations (see below).

This interaction and the resulting attachment of the molecule to the ascending step is very similar to the tendency of pyridine derivatives without peripheral phenyl groups, which attach to ascending metal step edges via their pyridyl groups.¹⁹ Similar type lateral N-metal interactions

are responsible also for the formation of metal-organic networks involving 2,4'-BTP^{20,21} or other pyridine derivatives.⁹ Based on DFT calculations of a Ag₂-pyridine cluster, Wu et al. determined a binding energy of -0.46 eV per pyridine-N-Ag₂ interaction,²² which is of the same order of magnitude as obtained for 2,4'-BTP stabilization by hydrogen bonds in ordered networks formed at higher coverages on Ag(100) (-0.46 eV per molecule).⁸ On the other hand, the N atoms in pyridine^{23,24} and 2,4'-BTP^{8,25} also interact with metal atoms which are located directly underneath them. Such kind of local interaction was found both theoretically and experimentally for adsorption of these molecules on different metal surfaces. DFT calculations revealed that the N atoms of pyridine favor the positions on top of metal atoms.^{23,24} For larger molecules like 2,4'-BTP this results in preferred azimuth orientations on the terraces of Ag(111) and Au(111).^{8,25} Similar trends were also found for 2,4'-BTP adsorption on Ag(100) terraces at higher coverages.¹⁵

Under thermodynamically controlled conditions, the preference for the configurations X_i is most simply explained by a chemical affinity of the upper terrace metal step edge to the aromatic rings. This closely resembles the behavior reported for benzene adsorption on Au(111), where STM imaging at 4 K (deposition also at 4 K), revealed a clear preference for adsorption at upper step edges.²⁶ That behavior was attributed to the nucleophilic character of benzene, which results in a preference for the positive partial charge at the upper step edge (Smoluchowski effect²⁷).²⁶ For the phenyl rings, which are chemically similar to benzene, one would expect a similar behavior. This explanation, however, does not explain why the remaining parts of most molecules obviously prefer to adsorb on the lower terrace. A possible reason, following the Smoluchowski picture, may be that the pyridyl rings themselves are electrophilic due to the electronegativity of their N atoms. Furthermore, we can assume that similar to the behavior of pyridine (see above) the pyridyl groups prefer to horizontally attach to ascending step edges, stabilized by the lateral N-Ag interactions. This explanation is supported by the observation that

none of the molecules adopts a configuration as shown in Figure 4c (X_3^*), where the mirror plane of the molecule is perpendicular to the step edge ($\delta=0^\circ$). In that configuration, N-Ag interactions are absent, at least for straight steps. Instead, rotation by an angle of $\delta=\pm 15^\circ$ seems to be most favorable, where both orientations were observed. Though this is not directly visible in our STM data, one may speculate that the molecules are actually attached to kink sites as depicted in Figure 4d, which allows to considerably enhance the number of Ag-N interactions. Looking at the rather irregular shape of the step edges in Figure 2a and Figure 3b, the presence of kink sites near the molecules is likely (see also Figure S1a in the supporting information). In Figure S1b, we illustrate the presence of kinks at bent steps. A clear decision on the importance and magnitude of the different energetic contributions to the preference of X_i configurations, however, is not possible on the basis of these experimental data alone.

Considering the high mobility of Ag surface atoms and steps, it is tempting to speculate on the origin of the kink configurations, i.e., whether the 2,4'-BTP ad molecules are bound to a preexistent kink configuration or whether this configuration is created during the attachment process, via an adsorbate induced restructuring of the step, to maximize the number of N-metal bonds. Such a re-structuring of steps was observed also for the adsorption of other large molecules on Cu(110).^{6,12,16,28} This question was investigated by measurements at different surface temperatures, with the sample placed in the STM during evaporation. When 2,4'-BTP is deposited on the surface at 300 K, the re-structuring could be due to detachment and attachment processes of Ag adatoms from and to the steps.²⁹ However, we performed also measurements at 124 K, where these processes are frozen on bare Ag(100). (The exact temperature for step immobilization on the clean Ag(100) surface is not known, but since Ag adatoms on Ag(100) terraces are already frozen at 160 ± 5 K, as determined from low energy ion scattering (LEIS) measurements,³⁰ the steps are definitely here frozen at 124 K.) The observation that the distribution of the arrangements of 2,4'-BTP molecules at steps is

comparable for deposition temperatures of 124 K, 156 K and 300 K (STM measurements always at 124 K), can be understood in the following picture: The distribution of adsorbed molecule-step configurations measured at 124 K reflects a thermodynamic equilibrium at a temperature somewhere around 130 - 140 K ('freezing temperature'). This is based on STM observations indicating that the lifetimes of adsorbed molecule-step configurations are in the ms range at 300 K, whereas at 130 K they are in the range of minutes. Neglecting that these are average values, which due to the different stabilities will differ for the various configurations, this means that similar distributions of configurations will be frozen during cool down from 300 K or 156 K, respectively. Obviously, even for deposition at 124 K, the time between deposition and STM imaging (minimum 1 h) and the remaining mobility, in particular of the more weakly bond configurations, are sufficient to reach a distribution of molecule-step configurations which within the statistical error is identical to that obtained during cool down.

In order to gain more insight into the physical origin for the preferred adsorption at step edges and specifically for the dominance of configuration X_3 , we performed DFT calculations. It is well-known that the adsorption of many aromatic molecules on surfaces is dominated by weak van der Waals forces which are not well-described in current DFT functionals.²⁴ In order to take these effects into account, we used a dispersion-corrected DFT (DFT-D) scheme.³¹ The adsorption of benzene (Figure 5a) and pyridine (Figure 5b) on Ag(100), Ag(711) and Ag(18 3 -2) was used to model the adsorption of phenyl and pyridyl moieties on flat terraces, steps and kink sites, respectively, of the Ag(100) surface since the first-principles description of the adsorption of the whole BTP molecule on metal surfaces is still computationally too costly. In order to explain the bonding nature in a more detailed fashion, the total adsorption energy E_{ad} (gained from DFT-D calculations) is split into two contributions stemming from covalent or electrostatic interactions ($E_{ad,DFT}$ from DFT calculations without dispersion correction) and contributions

caused by dispersive interactions ($E_{\text{ad,vdW}}$) (see Figure 5b). Further details about the calculations can be found in the supporting information.

The potential energy surface for the adsorption of benzene on Ag(100) shows a rather low corrugation ($\Delta E_{\text{ad}}=0.09$ eV, maximum difference between flat adsorbed benzene configurations in Figure 5a). Moreover, the adsorption at step edges is not strongly favored. This can be explained by the fact that the main contribution to the total adsorption energy ($E_{\text{ad}}=-0.58$ eV, leftmost image Figure 5a) stems from the dispersion interaction between benzene and the Ag surface ($E_{\text{ad,vdW}}=-0.53$ eV, not shown in Figure 5a).

Pyridine prefers an upright configuration (configuration I in Figure 5b) on Ag(100) terraces, in which the N atom is located atop of an Ag atom, although the difference with respect to flat lying geometry (Figure 5b, III) is low (0.12 eV). In that configuration, the electrostatic and covalent interactions ($E_{\text{ad,DFT}}$, Figure 5b, I) are maximized as an Ag-N interaction is formed. In contrast, the slightly smaller adsorption energy of flat adsorption geometries is dominated by dispersion interactions (Figure 5b, II-III). As the dispersion interactions get more important for larger molecules like 2,4'-BTP, we expect a clear preference for flat adsorption in the latter case, in full agreement with the experimental observations.

Comparing the adsorption energies of tilted pyridine on the terrace (II) and on the upper part of a step edge (IV) shows hardly any difference. Hence, there is essentially no stabilization by the different electronic properties at the step in this configuration. However, if pyridine is adsorbed flatly at the lower part of a step (V), it is stabilized by 0.27 eV compared to adsorption on a terrace in a flat orientation (III). In configuration (V), pyridine is adsorbed parallel to the terrace, it thus benefits from the dispersion interaction on the one hand and on the other hand its covalent/electrostatic interaction with the Ag atoms of the step is comparable to that in configurations (I), (II) and (IV), where the adsorbate is standing upright.

An additional stabilization of 0.1 eV is obtained if adsorption occurs at a kink site (VI). This is mainly due to the fact that the Pauli repulsion between the H atoms next to the N atom and the Ag atoms in the step edge is reduced and thus the absolute amount of $E_{\text{ad,DFT}}$ is increased.

These results clearly answer the question on the origin of the preferred step adsorption and preferential azimuth orientations raised before. The preference of pyridine to adsorb at steps or kink sites, perfectly explains the dominance of configuration X_3 observed in 2,4'-BTP adsorption experiments. In this configuration, two pyridyl rings and the pyrimidine are coordinated towards kink sites (Figure 4d). Considering the absence of a measurable stabilization for benzene adsorption on the upper step edge, the preference for configuration X_3 cannot be rationalized by a stronger interaction of the phenyl ring with the upper part of the terrace.

Hence, the driving force for BTP adsorption at step edges results from the interaction between the N atoms in the pyridyl moieties with the Ag atoms of the ascending step, with the new bond being parallel to the terrace surface. Additionally, covalent or electrostatic interactions are also present between the N atoms of an adsorbate and the atoms underneath them (see Figure 5b, III), though this contribution is less than that from bonds parallel to the surface, as well as dispersion interactions that stabilize the parallel configuration of the adsorbate on a terrace of a slightly tilted adsorption over a step. For Λ_i configurations, this leads to typically one N-Ag interaction. Only for the Λ_5 configuration, two interactions are possible for a specific kink configuration. The driving force for adsorption across the step edges (X_i configurations), which includes a shift of at least one ring to the upper terrace, originates from the same lateral interactions. In these configurations, the number of horizontal N-metal bonds per molecule is higher than in the Λ_i configurations, reaching up to 3 Ag-N bonds per molecule (X_3 configuration). Stabilization due to adsorption of phenyl rings on the upper terrace plays little role, it is rather considered to be a necessary move for increasing the horizontal Ag-N interactions.

The model described above is supported by measurements at higher 2,4'-BTP coverage, where 2,4'-BTP chains, stabilized by C-H...N hydrogen bonds, are formed. A model of these interactions between the molecules is shown in Figure S2 of the supporting information. These chains are in some cases connected to those parts of adsorbates at steps which rest at the lower side of steps (left-hand side of Figure 2a) via C-H...N-type hydrogen bonds.³²

We believe that these findings provide valuable insight into the role of defects such as steps and kinks in the adsorption and structure formation behavior of large organic molecules on metal surfaces, and on the competition between contributions from covalent/electrostatic interactions on the one hand and from dispersion interactions on the other hand. The relative strength of the interactions with these defects compared to the molecule-molecule interactions will be decisive for the formation of closed, defect-free molecular monolayers, which is particularly important when going to more realistic metal surfaces and metal-adsorbate systems.

CONCLUSIONS

Based on quantitative STM observations and DFT-D calculations, we have shown that preferred adsorption geometries of large adsorbates can exist at specific defect sites. In particular, ~79% of adsorbed 2,4'-BTP molecules at step edges of a Ag(100) surface are oriented with an angle of $\pm 15^\circ$ with respect to the $\langle 110 \rangle$ direction, while the rest of the adsorbates occurs in other well defined geometries. All adsorption geometries are governed by the trend for maximizing the number of interactions between intra molecular moieties and metal atoms in the surface parallel to the surface. In our model system, this leads to a pronounced preference for configurations where the adsorbates are bridged across the steps, with at least one aromatic ring located on the upper terrace, while the remaining ones are positioned on the lower terrace. For certain kink configurations, up to 3 Ag-N interactions are possible per molecule. Contributions from a preferential adsorption of phenyl moieties on the upper step edges can be neglected. The

resulting adsorption behavior is significantly different from that on atomically flat terraces. A similar behavior can be expected for other large adsorbates with peripheral moieties that are able to form interactions with metal atoms.

These findings provide valuable insight into the adsorption and structure formation behavior of large organic molecules at nano-scaled defect sites, which are present on every real metal surface. Moving away from idealized surfaces can yield important information when thinking about nano scaled functional devices based on organic adsorbates.

METHODS

The experiments were carried out in a standard UHV chamber with a base pressure $<3 \cdot 10^{-10}$ mbar. The Ag(100) surface (MaTeck GmbH) was cleaned by repeated cycles of Ar⁺ sputtering (0.5 keV, 4 μ A, 30 min) and annealing to 770 K. The cleanliness of the surface was checked by STM, showing ~ 200 nm wide terraces, curved monatomic steps and the absence of contaminations in atomic resolution images. 2,4'-BTP molecules were deposited by a Knudsen-type evaporator on the Ag surface (sample placed inside the STM and held at 124 K or 156 K). The deposition at 300 K sample temperature was done by a second evaporator in the load-lock system of the UHV chamber and the sample was subsequently cooled down inside the STM. Radiative heating of the sample by the evaporator is unlikely since the molecular beam from the evaporator passes thru a hole with a diameter of only ~ 1 mm and the sample is cooled very effectively during deposition (sample is in contact with the cooled copper block of the STM).

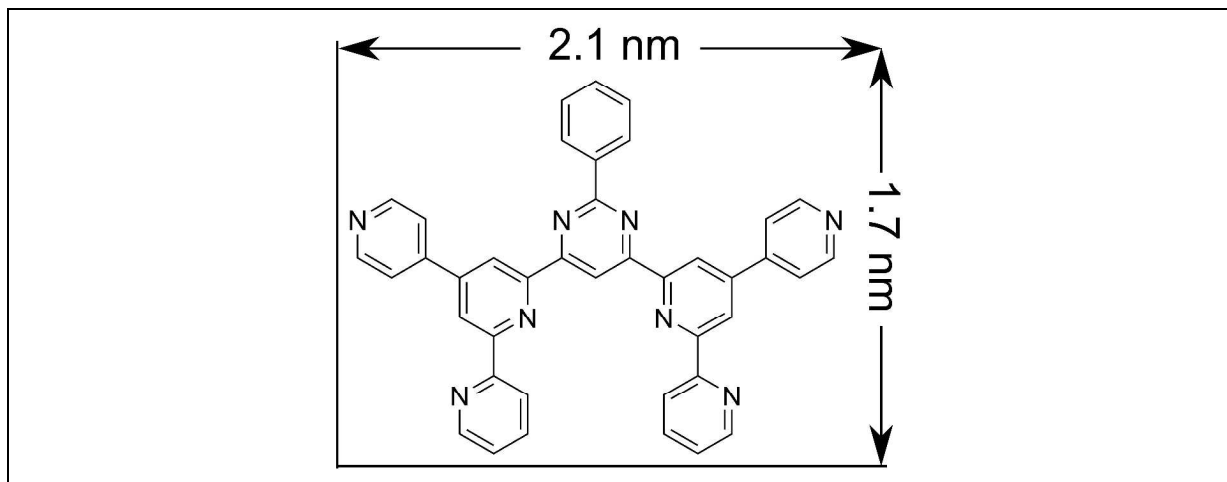
The surface was scanned with electrochemically etched tungsten tips in a liquid-nitrogen cooled Aarhus-type variable temperature STM (SPECS GmbH) in the constant current mode (tunnel conditions see figures).

Periodic DFT calculations were performed using the Vienna ab initio simulation package (VASP).³³ In order to account for electron-ion interactions, the projector augmented wave (PAW)

method^{34,35} was used. The van-der-Waals interaction was included in the DFT calculations using a dispersion-corrected DFT-D scheme.³¹ Further details of the calculations can be found in the supporting information.

ACKNOWLEDGEMENTS

We thank C. Meier, D. Caterbow and U. Ziener for providing the 2,4'-BTP material. This work was supported by the Deutsche Forschungsgemeinschaft via the Collaborative Research Center (SFB) 569. T. W. and C. N. acknowledge financial support by the Landesgraduiertenförderung Baden-Württemberg and by the German Academic Exchange Service (DAAD) via the RISE program, respectively.

**Figure 1**

Lewis formula of 2-phenyl-4,6-bis(6-(pyridine-2-yl)-4-(pyridine-4-yl)pyridine-2-yl)pyrimidine (2,4'-BTP).¹⁴ The sizes are with respect to the van der Waals radii of the perimeter atoms of the molecule.

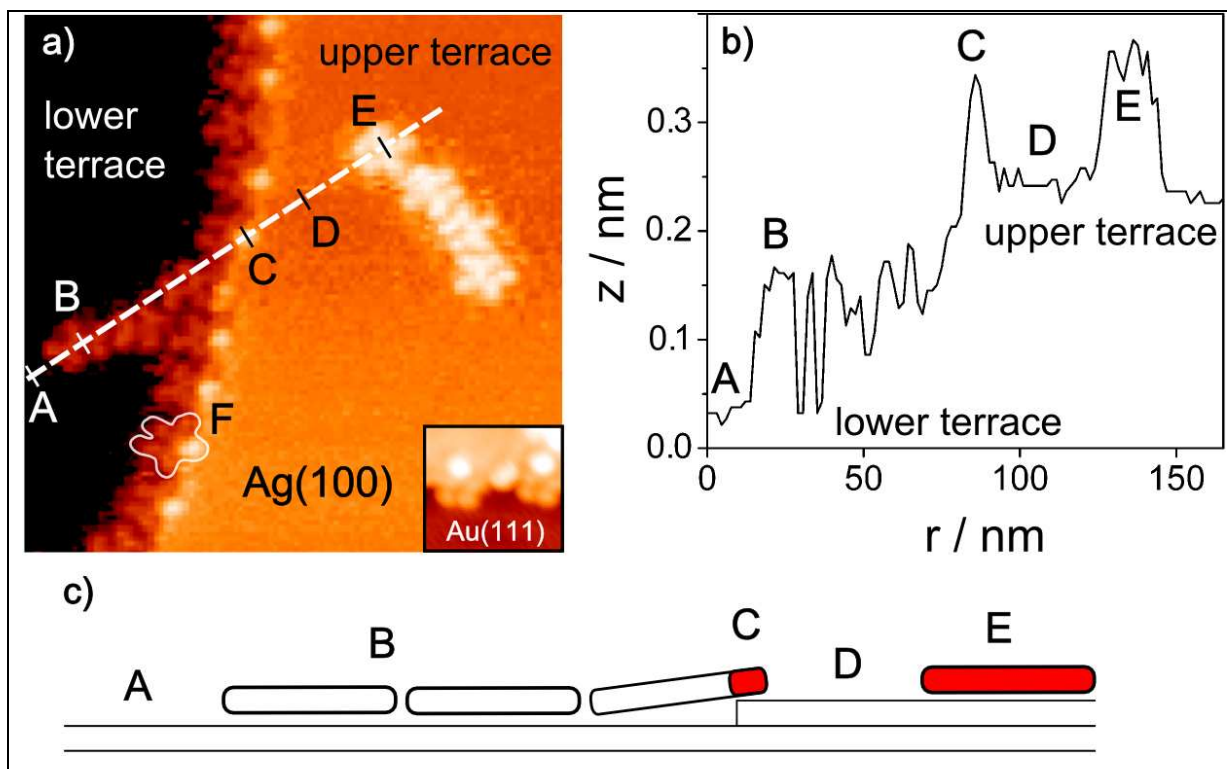
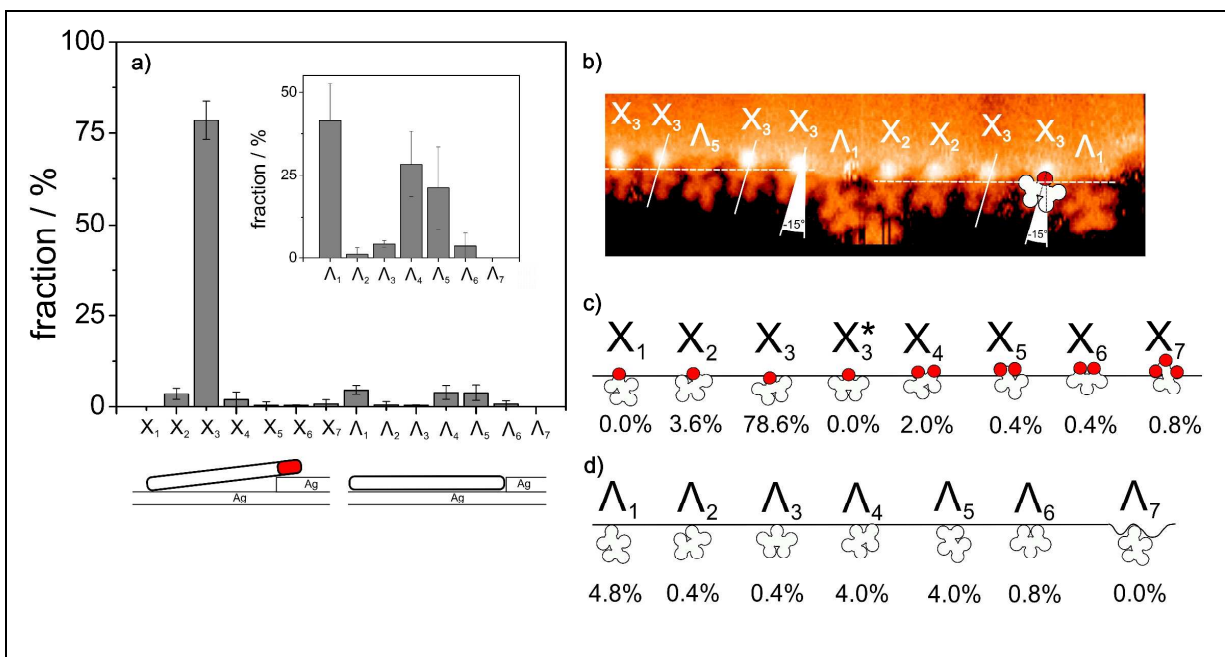


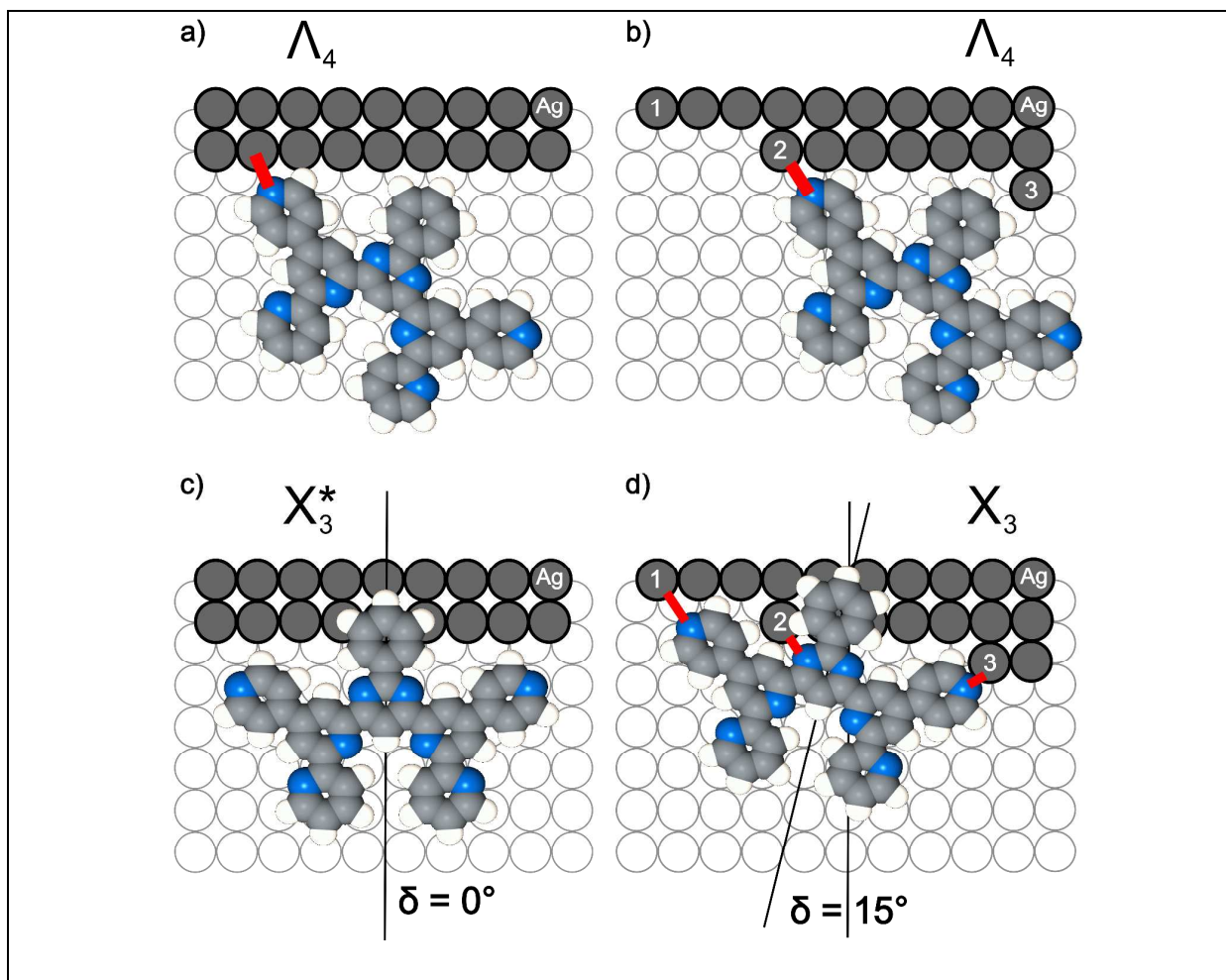
Figure 2

a) STM image of monatomic step on a Ag(100) surface saturated with 2,4'-BTP adsorbates, as well as two molecular chains located on the lower and upper terrace ($T=177\text{K}$, $I_T=52\text{pA}$, $U_T=-2.22\text{V}$, $16\times 16\text{ nm}^2$). The inset shows a similar phenomenon for 2,4'-BTP on a Au(111) step edge ($T = 142\text{K}$, $I_T = 50\text{pA}$, $U_T = -2.02\text{V}$, $4\times 4\text{ nm}^2$). b) Cross-section along the dashed line in the STM image (a). z is the apparent height position of the STM tip, which is higher if the tip is located above an adsorbate or on an upper step edge. c) Schematic drawing (side view) of the adsorption configuration along the A-E in b) (red = on upper terrace). The points A-E mark the same points in (a), (b) and (c). A: lower terrace (bare Ag), B: molecules on lower terrace, C: position of the phenyl ring of a typical molecule (type X_3) on the step edge, D: upper bare Ag terrace, E: molecule on the upper terrace. C and E have similar apparent heights compared to D. For F, a molecule bridging the step is marked exemplarily.

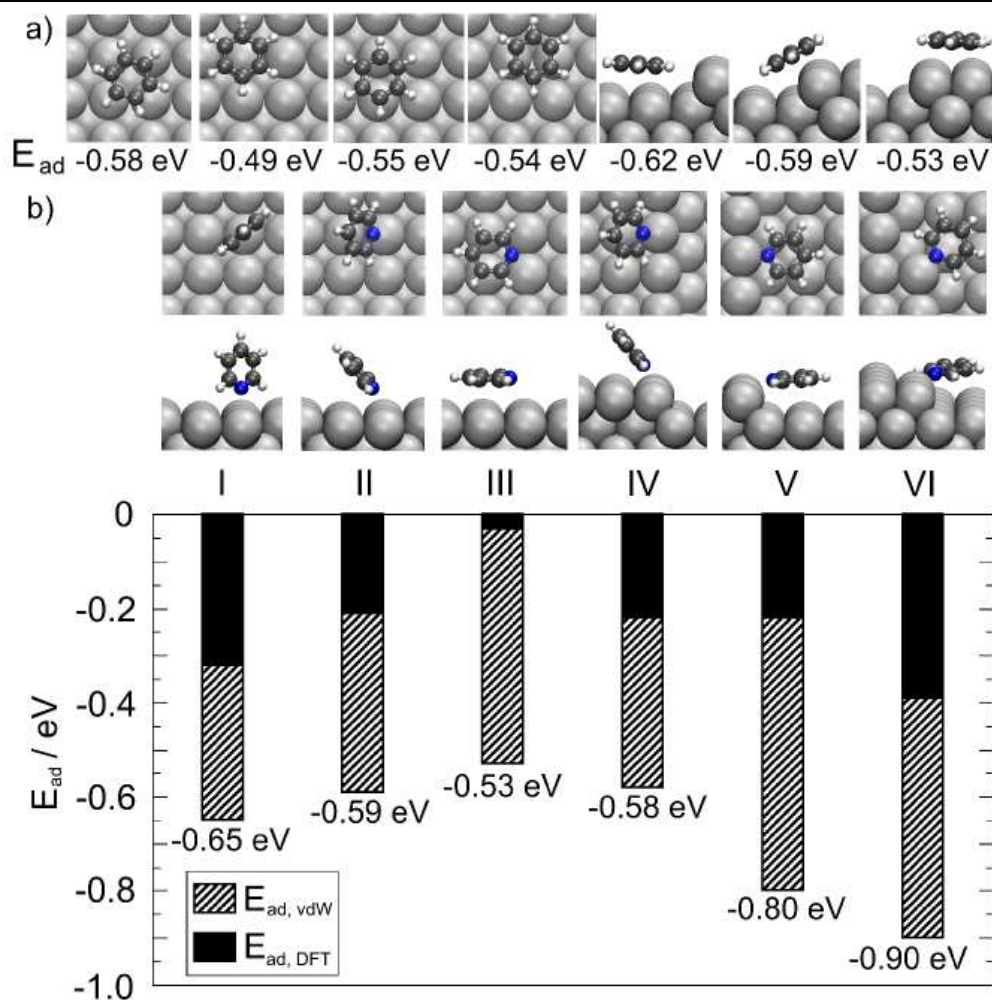
**Figure 3**

Statistic evaluation of the experimentally found configurations of 2,4'-BTP molecules at step edges on Ag(100); bright protrusions in the STM images are marked red in the model. 252 molecules at steps were evaluated.

a) Histogram of all observed configurations (X_i and Λ_i). The inset shows the histogram only for the configurations Λ_i . The error bars are 95% confidential intervals. b) STM image showing different exemplary configurations at a step edge. c) Schematic representation of configurations $X_1 - X_7$ with pyridyl and/or phenyl rings of 2,4'-BTP lying on step edges, while the rest of the adsorbates is located at the lower terrace. d) Configurations $\Lambda_1 - \Lambda_7$ where the adsorbate is fully located on the lower terrace.

**Figure 4**

Models of 2,4'-BTP molecules adsorbed at (a,b) or across (c,d) linear (a,c) and kinked (b,d) steps on Ag(100) (upper terrace metal atoms: dark grey, lower terrace metal atom: white, C: light gray, N: blue, H: white). a,b) Adsorption at the ascending step, with the admolecule fully located on the lower terrace, in configurations Λ_4 . c,d) Adsorption across the ascending step, with c) configuration (X_3^*) with $\delta=0^\circ$, which was not observed, and d) energetically favorable configuration X_3 of adsorbed 2,4'-BTP with the phenyl ring on the upper terrace of the Ag(100) surface. Ag atoms 2 and 3 represent the kink atoms. The latter configuration is stabilized by 3 N-Ag interactions (marked red) involving Ag atoms 1, 2 and 3 and the neighboring pyridyl moieties.

**Figure 5**

Adsorption energies from DFT-D calculations of a) benzene and b) pyridine on Ag(100), Ag(711) and Ag(18 3 -2). The first four images in (a) show a top view of different adsorption configurations of benzene on a Ag(100) terrace, the last three images correspond to side views of benzene adsorbed in different configurations at a step edge (Ag(711)). The energies shown in (a) represent total adsorption energies. (b) shows the adsorption geometries of pyridine on a terrace (I-III, Ag(111)), step edge (IV,V, Ag(711)) and kink site (VI, Ag(18 3 -2)) considered in the calculations. The upper row of images represents top views, the lower one side views, respectively. In (b) the total adsorption energies are split into dispersion interactions $E_{ad, vdW}$ and covalent interactions $E_{ad, DFT}$.

References

1. C. W. Tang, S. A. VanSlyke, *Appl. Phys. Lett.*, 1987, **51**, 913.
2. S. R. Forrest, *Chem. Rev.*, 1997, **97**, 1793.
3. F. Rosei, M. Schunack, N. Yoshitaka, P. Jiang, A. Gourdon, E. Laegsgaard, I. Stensgaard, C. Joachim, F. Besenbacher, *Prog. Surf. Sci.*, 2003, **71**, 95.
4. S. de Feyter, F. de Schryver, *Chem. Soc. Rev.*, 2003, **32**, 139.
5. F. Cacialli, P. Samorì, C. Silva, *Mat. Today*, 2004, **7**, 24.
6. F. Rosei, M. Schunack, P. Jiang, A. Gourdon, E. Laegsgaard, I. Stensgaard, C. Joachim, F. Besenbacher, *Science*, 2002, **296**, 328.
7. J. V. Barth, *Ann. Rev. Phys. Chem.*, 2007, **58**, 375.
8. H. E. Hoster, M. Roos, A. Breitruck, C. Meier, K. Tonigold, T. Waldmann, U. Ziener, R. J. Behm, *Langmuir*, 2007, **23**, 11570.
9. S. L. Tait, A. Langner, N. Lin, S. Stepanow, C. Rajadurai, M. Ruben, K. Kern, *J. Phys. Chem. C*, 2007, **111**, 10982.
10. P. Ruffieux, K. Palotás, O. Gröning, D. Wasserfallen, K. Müllen, W. A. Hofer, P. Gröning, R. Fasel, *J. Am. Chem. Soc.*, 2007, **129**, 5007.
11. M. Treier, P. Ruffieux, R. Schillinger, T. Greber, K. Müllen, R. Fasel, *Surf. Sci.*, 2008, **602**, L84-L88.
12. M. Yu, W. Xu, Y. Benjalal, R. Barattin, E. Laegsgaard, I. Stensgaard, M. Hliwa, X. Bouju, A. Gourdon, C. Joachim, T. R. Linderoth, F. Besenbacher, *Nano. Res.*, 2009, **2**, 254.
13. B. Hammer, O. H. Nielsen, J. K. Nørskov, *Catal. Lett.*, 1997, **46**, 31.
14. U. Ziener, J. M. Lehn, A. Mourran, M. Möller, *Chem. Eur. J.*, 2002, **8**, 951.
15. T. Waldmann, C. Nenon, H. E. Hoster, R. J. Behm, *Phys. Chem. Chem. Phys.*, 2011, **13**, 20724.
16. M. Schunack, F. Rosei, Y. Naitoh, P. Jiang, A. Gourdon, E. Lægsgaard, I. Stensgaard, C. Joachim, F. Besenbacher, *J. Chem. Phys.*, 2002, **117**, 6259.
17. J. Coraux, A. T. N'Diaye, M. Engler, C. Busse, D. Wall, N. Buckanie, F. J. Meyer zu Heringdorf, R. van Gastel, B. Poelsema, T. Michely, *New J. Phys.*, 2009, **11**, 23006.
18. K. Donner, P. Jakob, *J. Chem. Phys.*, 2009, **131**, 164701.
19. S. L. Tait, Y. Wang, G. Costantini, N. Lin, A. Baraldi, F. Esch, L. Petaccia, S. Lizzit, K. Kern, *J. Am. Chem. Soc.*, 2008, **130**, 2108.

20. A. Breittruck, H. Hoster, C. Meier, U. Ziener, R. J. Behm, *Surf. Sci.*, 2007, **601**, 4200.
21. A. Breittruck, H. E. Hoster, R. J. Behm, *J. Phys. Chem. C*, 2009, **113**, 21265.
22. D. Y. Wu, M. Hayashi, Y. J. Shiu, K. K. Liang, C. H. Chang, Y. L. Yeh, S. H. Lin, *J. Phys. Chem. A*, 2003, **107**, 9658.
23. A. Bilic, J. R. Reimers, N. S. Hush, *J. Phys. Chem. B*, 2002, **106**, 6740.
24. K. Tonigold, A. Groß, *J. Chem. Phys.*, 2010, **132**, 224701.
25. T. Waldmann, R. Reichert, H. Hoster, *Chem. Phys. Chem.*, 2010, **11**, 1513.
26. E. C. H. Sykes, B. A. Mantooh, P. Han, Z. J. Donhauser, P. S. Weiss, *J. Am. Chem. Soc.*, 2005, **127**, 7255.
27. R. Smoluchowski, *Phys. Rev.*, 1941, **60**, 661.
28. R. Otero, F. Rosei, Y. Naitoh, P. Jiang, P. Thostrup, A. Gourdon, E. Lægsgaard, I. Stensgaard, C. Joachim, F. Besenbacher, *Nano Lett.*, 2004, **4**, 75.
29. S.-L. Chang, J.-M. Wen, P. A. Thiel, S. Günther, J. A. Meyer, R. J. Behm, *Phys. Rev. B*, 1996, **53**, 13747.
30. M. H. Langelaar, M. Breeman, D. O. Boerma, *Surf. Sci.*, 1996, **352-354**, 597.
31. S. Grimme, J. Antony, S. Ehrlich, H. Krieg, *J. Chem. Phys.*, 2010, **132**, 154104.
32. C. Meier, U. Ziener, K. Landfester, P. Wehrich, *J. Phys. Chem. B*, 2005, **109**, 21015.
33. G. Kresse, *Phys. Rev. B*, 1996, **54**, 11169.
34. P. E. Blöchl, *Phys. Rev. B*, 1994, **50**, 17953.
35. G. Kresse, D. Joubert, *Phys. Rev. B*, 1999, **59**, 1758.

